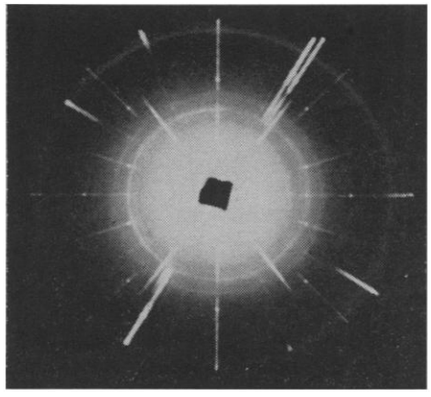

Fig. 1. Precession pattern ($\mu = 16°$, Pd-filtered Ag radiation) of the $hk0$ level of ice VI at room temperature. The heavy diagonal streaks are from the diamonds and the rings are from the metal gasket.

tained at room temperature and approximately 9 kb by means of a modified, opposed diamond-anvil pressure cell (*1*). Pressure was applied to distilled water confined between the diamond anvils by a metal gasket. On initial application of pressure, ice VI was formed in a polycrystalline mass. To eliminate the polycrystalline character, pressure was reduced until only one crystallite remained. This crystallite was grown by slowly reapplying pressure until it filled the entire pressure chamber (*2*). By means of a modified precession camera incorporating the pressure cell, single-crystal patterns of ice VI were obtained with Pd-filtered Ag radiation ($\lambda = 0.5609$ Å). Silver Kα radiation was employed to minimize absorption effects and to decrease the size of the reciprocal lattice, thus enabling us to obtain more data. A detailed description of the apparatus will be published elsewhere.

Table 1. Observed and calculated spacings.

Spacing, 10^{-8}cm		*hkl*
Obs.	Calc.	
4.3	4.3	111*
3.6	3.6	012
3.4	3.5	210
3.12	3.08	020
2.91	2.93	021*
2.75	2.75	121
2.63	2.67	301
2.51	2.51	022
2.43	2.42	203
2.21	2.22	004*
2.10	2.09	400
2.01	2.00	031*
1.97	1.97	204
1.85	1.85	230
1.75	1.76	124
1.64	1.64	205
1.56	1.57	502*
1.48	1.48	006
1.44	1.44	142*
1.41	1.42	513
1.37	1.37	424
1.34	1.34	035
1.30	1.30	612
1.26	1.26	107
1.21	1.21	151
1.14	1.14	712
1.104	1.104	108
1.084	1.081	615*
1.050	1.049	535*
1.010	1.009	642

* Multiple line, only one possible index is given.

Cone-axis photographs along c and precession patterns of $hk0$ and $hk1$ were obtained. Also, photographs of patterns containing b^* with $h0l$ ($h \neq 0$) were taken. Because of the preferential direction of growth of the crystal and the somewhat restricted movements of the pressure cell itself, no patterns containing c^* were observed. To date, information on the c-axis has been obtained only from cone-axis and mixed-index photographs. The cell constants derived from these data are $a = 8.38 \pm 0.05$ Å, $b = 6.17 \pm 0.05$ Å, and $c = 8.90 \pm 0.15$ Å (*3*). These values together with the density data reported by Bridgmen (*4*) yield $Z = 20$. The systematic absences are $hk0$, $h = 2n + 1$ and $0k0$, $k = 2n + 1$ and indicate the orthorhombic aspect $P^{**}a$.

Figure 1 shows a typical precession pattern of the $hk0$ level of ice VI. The μ angle was 16°. The heavy diagonal streaks arise from the diamonds and the diffraction rings from the metal gasket.

McFarlan (*5*) reported the first x-ray diffraction data on the high-pressure forms of ice. He conducted his x-ray diffraction studies at 1 bar and at low temperature—the low temperature being used to "freeze in" the structures formed at high pressure. No diffraction data were reported for ice VI—the dense form of ice in equilibrium with water at room temperature and approximately 9 kb—but he noted that the data were indicative of low symmetry and that the powder pattern could not be indexed readily. Recently, Bertie, Calvert, and Whalley (*6*) have reported diffraction data for all the known ice structures with measurements on the high-pressures phases being made at 1 bar and 90°K. They also have not indexed the diffraction data on polycrystalline ice VI.

The cell constants obtained here can be used to index the pattern of polycrystalline ice VI in the metastable state reported by Bertie, Calvert, and Whalley to within the probable errors arising from the differences in temperatures and pressures of the two experiments. The indexing is shown in Table 1.

As a result of work with ice VI, modifications of the pressure-cell are being considered to facilitate greater freedom of orientation of the crystals.

S. Block
C. W. Weir
G. J. Piermarini
National Bureau of Standards, Washington, D.C.

References and Notes

1. C. E. Weir, E. R. Lippincott, A. Van Valkenburg, E. N. Bunting, *J. Res. Nat. Bur. Std. A* **63**, 55 (1959).
2. This technique was developed by A. Van Valkenburg and has not been published.
3. The uncertainties given are based on experience with the equipment used. Errors for the a and b axes are smaller that that for the c axis because the former were measured directly.
4. P. W. Bridgman, *Proc. Am. Acad. Arts Sci.* **47**, 441 (1911).
5. R. L. McFarlan, *J. Chem. Phys.* **4**, 60, 253 (1936).
6. J. E. Bertie, L. D. Calvert, E. Whalley, *ibid.* **38**, 840 (1963); *Canad. J. Chem.* **42**, 1373 (1964).

18 January 1965

Radioactivity: Detection of Gamma-Ray Emission in Sediments in situ

Abstract. *A probe for measuring emission of γ-rays in sediments* in situ *in water depths to about 35 meters was used to measure radioactivity in the Columbia River estuary and Oregon coastal areas. This technique offers some advantage over methods in which sediment samples are collected at sea and returned to the laboratory for radioanalysis.*

Because artificial radioactivity has been present in quantity only since 1944, man-made radionuclides are confined to the most recently deposited marine sediments. This thin surface layer of sediment, though of greatest interest, is most difficult to remove in its undisturbed state in quantities sufficient for radioanalysis. Coring devices cause the least disturbance in the sample, but the proportion of surface sediments recovered is small. Both dredged and grabbed samples contain relatively large proportions of surface sediments, but older, less radioactive sediments are often mixed into the desired sample and confound the analysis. Also some of the finer-grained sediments are likely to be washed out of such samples as they are brought to the surface. The greater

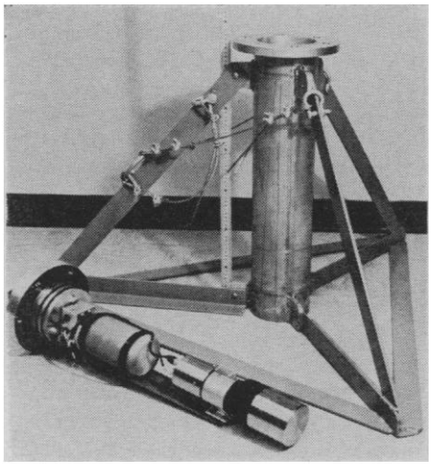

Fig. 1. Sediment probe for measuring γ-ray emission in the field.

ratio of surface area to volume of these smaller particles possibly causes them to contain an appreciable fraction of the radioactivity.

An *"in situ"* probe should obviate some of the problems associated with the measurement of radioactivity in marine sediments, although it, too, might disturb the fine material to a certain extent when it touches bottom. The detector rests on the bottom and "views" the upper surface of the ocean floor; that is, the top few centimeters below the sediment-water interface (*1*). The water contains K^{40} but otherwise is low in radioactivity, and contributes little to the γ-ray emission spectrum.

A number of investigators have used γ-ray probes to measure radioactivity in the field. A probe developed by Le Vine (*2*), which was towed behind the U.S. Coast Guard cutter *Taney* in the vicinity of Rongelap, probably represents the first major effort to measure artificial radioactivity in the ocean directly. Proctor *et al.* (*3*) and Gross *et al.* (*4*) used probes to measure γ-ray emission in marine waters. In California, Klingeman and Kaufman (*5*) mounted a detector on an underwater sled to survey fallout radionuclides in the bottom of San Pablo Bay. However, they report that individual radioisotopes were not identified in this program.

We have tested a new probe in water depths as great as 35 m at a number of locations in the Columbia River estuary and in the ocean nearby. This probe was based on ideas originated by the workers mentioned above, but the design was modified to adapt it to measurement of γ-ray emission in sediments.

The detector, a NaI(Tl) crystal (7.5 by 7.5 cm) with attached photomultiplier, plus preamplifier and batteries, is sealed in an aluminum pipe 14 cm in diameter, 63.5 cm long, and 0.635 cm thick. Samples of Cr^{51} counted in the laboratory with no absorber and with a 0.635-cm thickness of aluminum show that the counting rate for Cr^{51} (0.32 Mev) is reduced only about 20 percent by the aluminum housing. There is, of course, even less attenuation of the higher-energy γ-ray emitters such as K^{40} (1.46 Mev). Measurements of radionuclides of several energies showed that the system is linear up to 1.46 Mev. The detector is molded in styrofoam to reduce thermal and physical shock. A tripod orients the detector on the bottom so that the positioning is generally reproducible (Fig. 1). Scuba divers, who observed the device in operation in initial tests, reported that the probe showed no tendency to tip. However, a mercury switch shuts off the power in the event the probe is appreciably tilted. Thus, proper orientation of the probe while "counting" is insured, and the batteries can be conserved by simply tipping the probe on its side when not in use.

Signals from the probe are carried to an ND-130 AT 512 channel spectrometer in the boat through 0.318-cm steel-armored single-conductor cable (Amergraph, U.S. Steel). The γ-ray spectra are recorded on Tally punch tape for laboratory analysis. A portable winch raises and lowers the probe by means of the single cable. Small (up to 9.6 m) fishing boats were chartered for river tests, and a portable generator furnished power to the spectrometer. The research vessel *Yaquina* (54 m) was used for off-shore work, including that reported herein.

A sample spectrum of fine sand (Fig. 2*a*), under 21 m of water in the Pacific Ocean 4.8 km off the mouth of the Columbia River, reveals several radionuclides from the Hanford, Washington, nuclear reactors, and naturally radio-

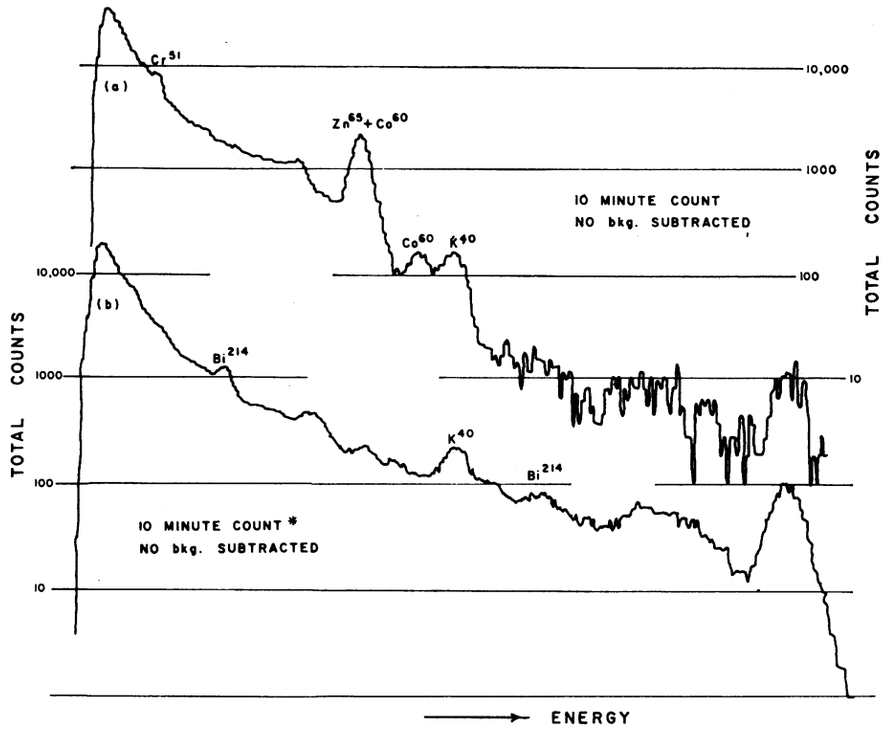

Fig. 2. *a*, Gamma-ray spectrum of fine sand beneath 21 m of water, 4.8 km off the mouth of the Columbia River. Counting time 10 minutes, no background subtracted, 11 October 1963. Chromium-51, zinc-65, and cobalt-60 are principally from Hanford, Washington, and potassium-40 and bismuth-214 (radium C) are naturally occurring. The high-energy peak (lower right) has not been positively identified, but appears to be associated with the thorium series. *b*, Similar spectrum of coarse sand and gravel beneath 30 m of water, 1.6 km off Newport, Oregon, 18 November 1964. Counting time was 40 minutes, no background subtracted, but spectrum was normalized to 10 minutes (all counts multiplied by 0.25) for comparison with Fig. 2*a*. There is less scatter in the high-energy portion of this spectrum as a result of both better statistics from the longer counting time and an actual higher counting rate from the emitting substance whose peak falls at the right edge of the spectrum.

active K^{40}. Although the same radionuclides were reported in core samples from this general area (*6*), the *in situ* spectra are clearly superior. The large "sample size" assures an increased counting rate that more than compensates for the loss of detail resulting from the effects of the water on the γ-ray photons.

Comparison of a spectrum of coarse sand and gravel, in 30 m of water 1.6 km off Newport, Oregon (Fig. 2*b*), shows no radionuclides resulting from operations at the Hanford laboratories. The plume of the Columbia River does not normally move into this area, although marine animals taken here contain Zn^{65} (*7*). Most deposits of silts and clays in the northeast Pacific Ocean, which might have larger amounts of artificial radioactivity than sands and gravels, are beyond the present range of our probe. Range is restricted by the 54-m cable used in these tests, but Riel (*8*) has shown that longer cable lengths are feasible. The probe housing was designed for and tested at much greater pressures, and the only modifications required are in the cable length and associated electronics. These modifications are in progress and should let us work down to about 400 m.

Our interest lies in the relationship of the radioactivity of animals to that of their environment. Analysis techniques for animals are relatively simple, since the specific activity of the samples can be increased by ashing, with the ash counted in the well of a NaI(Tl) crystal (12.5 by 12.5 cm) in the laboratory. There is no easy comparable method of concentrating the radioactivity in sediment samples. The difficulties inherent in the collection and subsequent radioanalysis of sediments seem to make methods of probing *in situ* worthy of further effort.

DAVID JENNINGS
NORMAN CUTSHALL
CHARLES OSTERBERG
Department of Oceanography, Oregon State University, Corvallis

References and Notes

1. The actual depth to which the probe "sees" depends on both the energy of the γ-ray emitters and the density of the matrix material. Therefore, the effective size of the sample would be less for Cr^{51} (0.32 Mev) than for K^{40} (1.46 Mev).
2. J. H. Harley, Ed., *Operation* Troll: *Joint preliminary report* (HASL, U.S. Atom. Energy Comm., New York Operations Office, NYO 4656, April 1956).
3. C. M. Proctor, E. Papadopulos, R. H. Firminhac, *Limnol. Oceanogr.* **7**, 280 (1962).
4. M. G. Gross, C. A. Barnes, G. K. Riel, in preparation.
5. P. C. Klingeman and W. J. Kaufman, "Transport of radionuclides with San Francisco Bay sediments," Progress Report 1961-1962 Water Year. *Sanitary Eng. Res. Lab. Rep.* No. 63-7, (Univ. of California, Berkeley, 1963), p. 70.
6. C. Osterberg, J. Byrne, V. Kulm, *Science* **139**, 916 (1963).
7. C. Osterberg, J. Pattullo, W. Pearcy, *Limnol. Oceanogr.* **9**, 249 (1964).
8. G. K. Riel, *Electronics* **36**, No. 10, 56 (8 Mar. 1963).
9. Support from U.S. AEC contract AT(45-1)1750 and PHS training grant 1T1-WP-59-01. The data are a result of thesis research for a master's degree from Oregon State University. We thank R. S. Mesecar and W. E. Bales for design of the electronic circuitry and suggestions for waterproofing the probe.

23 February 1965

Kink-Bands: Shock Deformation of Biotite Resulting from a Nuclear Explosion

Abstract. *Microscopic examination of granodiorite samples from the shock region around a nuclear explosion reveals sharply folded lens-shaped zones (kink-bands) in the mineral biotite. Fifty percent of these zones are oriented approximately 90° to the direction of shock-wave propagation, but other zones are symmetrically concentrated at shear angles of 50° and 70° to the direction of shock-wave propagation.*

In 1962, a 5.2-kiloton nuclear device was detonated in the granodiorite of the Climax stock, Nevada Test Site (Hardhat event). Deformation of biotite in the form of sharply folded lens-shaped zones (kink-bands) was observed by microscopic examination of samples affected by the shot. As a basis for defining explosion-produced effects, samples taken prior to the detonation were examined and compared with those taken after the shot (postshot samples). The locations in the reentry tunnel where the postshot samplings were made and the drill core are shown in Fig. 1.

All thin sections cut from the six samples in the reentry tunnel were oriented by having the planar dimension of the section parallel to a radius drawn from the shot point. Although the orientation for most sections cut from the postshot drill core was not known (because of rotation of the sample in the core barrel during drilling), sections from the four samples C_8, C_9, C_{10}, and C_{11} could be oriented parallel to a radius from the shot point.

Of the ten oriented postshot sections only the eight within the shock zone (*1*) displayed kink-bands (Fig. 1). These eight were examined for preferred directions of kink-bands. Of the 110 observed kink-bands in the oriented sections, 50 percent were oriented with the long axis of the lens at 90° ± 5° to a radius drawn from the shot point (Fig. 2*A*). Approximately 12 percent and 10 percent were oriented with the long axis of lens at 50° ± 1° and 70° ± 1°, respectively, from the radius (Fig. 2*B*).

Because only the eight oriented samples within the shock zone showed kink-bands, the explosion-produced shock wave was probably the (compressive) stress which formed the kink-bands. The shock wave passes spherically outward from the shot point so that its front moves along radii drawn from the shot point. The kink-band orientation can thus be related to the direction of wave propagation. The unoriented sections can be oriented by assuming that the greatest percentage of kink-bands is normal to the direction of shock-wave propagation.

A total of 701 kink-bands from oriented and unoriented sections were counted. Their frequencies and orientations with respect to the shock wave are shown on Fig. 3. The relative frequencies of the principal orientations for the unoriented sections are the same as those from the oriented sections. This suggests that the method for deducing the direction of shock-wave propagation in unoriented sections is not greatly in error.

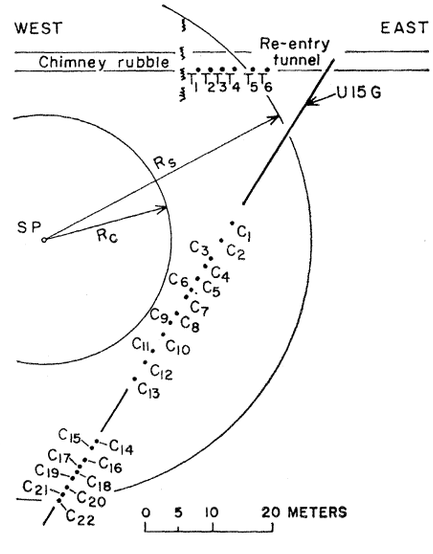

Fig. 1. Cross-sectional diagram in the vicinity of the Hardhat event showing the reentry tunnel, postshot drill hole (U15G), shock-zone radius (R_s), cavity radius (R_c), shot point (SP), and sample locations in the tunnel ($T_1 \cdots T_6$) and drill hole ($C_1 \cdots C_{22}$).